KfK 4474
Oktober 1988

Design of a Fast Electron Beam Scanning System for Compact Synchrotron Light Sources

H. O. Moser, H. Lehr
Institut für Kernverfahrenstechnik

Kernforschungszentrum Karlsruhe

KERNFORSCHUNGSZENTRUM KARLSRUHE

Institut für Kernverfahrenstechnik

KfK 4474

Design of a Fast Electron Beam Scanning System for Compact Synchrotron Light Sources

H.O. Moser, H. Lehr *)

*) BESSY GmbH, Berlin

Kernforschungszentrum Karlsruhe GmbH, Karlsruhe

Kernforschungszentrum Karlsruhe GmbH
Postfach 3640, 7500 Karlsruhe 1

ISSN 0303-4003

Entwurf einer Vorrichtung zum schnellen Kippen des Elektronenstrahls in kompakten Synchrotronstrahlungsquellen

Zusammenfassung

Der Entwurf eines Elektronenstrahl-Kipp-Systems für kompakte Speicherring-Synchrotronstrahlungsquellen wird beschrieben. Die Haupteigenschaften sind eine Kippfrequenz von 100 Hz und eine Winkelamplitude von ± 5 mrad. Mit zwei verschiedenen Anordnungen von Kippdipolen kann der Kipp auf eine Zelle beschränkt werden, wozu 4 Kippdipole benutzt werden, oder er kann periodisch in jedem Ablenkmagnet wiederholt werden mittels zwei Kippdipolen pro Zelle. Kombinationen dieser Grundanordnungen sind möglich. Die Lage des Knotens des kippenden Elektronenstrahls kann auf den maximalen Kippwinkel optimiert werden, indem die magnetische Flußdichte in verschiedenen Kippdipolen leicht verstimmt wird. Die Kippdipole haben die Form von H-Magneten und sind aus geblechtem Eisen. Ihre Spalthöhe beträgt 68 mm. Sie werden durch Netzgeräte versorgt, in denen schnelle Transistor-Brückenschaltungen durch frei programmierbare Funktionsgeneratoren gesteuert werden, die ihrerseits den dreiecksförmigen Strom-Zeit-Verlauf bis auf eine Abweichung von weniger als 0.1 % darstellen können, mit Ausnahme einer Umgebung von 1 % der Periodendauer um die Dreiecksspitze herum. Abschätzungen zum Einfluß des Strahlkipps auf die Quanten- und auf die Coulomb-Lebensdauer deuten auf akzeptable Lebensdauer-Verminderungen hin unter der Voraussetzung, daß der minimale Abstand zwischen der verformten Sollbahn und der begrenzenden Öffnung etwa 6 Standardabweichungen der räumlichen Elektronenverteilung übersteigt.

Design of a Fast Electron Beam Scanning System for Compact Synchrotron Light Sources

Abstract

The design of an electron beam scanning system for compact storage ring synchrotron light sources is described. The main features are a scan frequency of 100 Hz and an angular amplitude of ±5 mrad. Two different configurations of scan dipoles allow to confine the scan to one cell using 4 dipoles or to repeat the scan periodically in each bending magnet by means of 2 scan dipoles per cell. Combinations of these basic configurations are possible. The location of the node of the pivoting electron beam can be optimized with respect to the maximum scan angle by slightly unbalancing the field strength in different scan dipoles. The scan dipoles are H-shaped magnets made from laminated iron. Their gap width is 68 mm. They are powered by fast transistor-bridge power supplies which are controlled by freely programmable function generators capable to realize a triangular current waveform with a deviation of less than 0.1 % except for a 1 % neighbourhood of the apex. Estimates of the influence of the scanning on both quantum and Coulomb lifetime indicate acceptable lifetime reductions provided the minimum distance between distorted closed orbit and aperture exceeds about 6 standard deviations of the spatial electron distribution.

Introduction

The scanning of the electron beam of synchrotron light sources has been proposed and investigated previously /1-4/ in order to enlarge the field illuminated by synchrotron radiation. One of the main interests to do that is to avoid mechanical stepping of large wafers in X-ray lithography. Furthermore, the local divergence angle of the radiation on the target may be reduced from the total divergence angle in the synchrotron light beam to the maximum local one. Finally, with powerful synchrotron light sources exposure time may be shortened by a factor equal to the ratio between the widths of both target and irradiated region.

The scanning will influence not only the lithography on the target, but also the storage ring operation. As a consequence, a scanning system must be designed to allow investigation of lithographic issues over a wide range of parameters while minimizing unwanted effects on the electron beam and the storage ring. These effects include beam lifetime reductions due to the periodic aperture variation, unwanted closed orbit distortions caused by dynamic mismatch of the scan dipoles as well as radiative and particle heat load of the cryogenic structure. For polymethylmethacrylate (PMMA) as a resist the thermal diffusivity is about 1×10^{-3} cm^2/s. Then, a 0.5 mm thick slab of PMMA fastened to a heat sink on one side has a thermal relaxation time of the order of 1 s. In order to shorten exposure time by scanning the dwell time of the synchrotron light beam on a given target point should be significantly less than the thermal relaxation time. Furthermore, the faster the scan the less the irradiated target will be repeatedly deformed by thermal cycling.

Accordingly, the scanning system presented is designed to have a maximum scan frequency of 100 Hz. In order to have a useful scan height of 10 cm in a distance of 10 m the maximum angular scan amplitude is ± 5 mrad. Different configurations of scan dipoles are described which allow to scan simultaneously in all bending magnets, or to restrict the scan to one or several preselected regions, or to shift the node of the pivoting electron beam along the real closed orbit. The design of a scan dipole with a sufficiently large aperture and a rapid time response as well as the necessary fast power supplies and precise function generators are discussed. Finally, a calculation of quantum and Coulomb lifetimes taking into

account the periodic reduction of aperture indicates that this effect is acceptable.

Restricted scan

The lattice of the superconducting storage ring synchrotron radiation source (KSSQ) planned at Karlsruhe for deep-etch microlithography according to the LIGA process /5/ is shown in fig. 1. Compared to previous designs /4/ it has been modified by including standard quadrupoles of greater length and by increasing the lengths of the straight sections to accommodate a 3-cell RF cavity and optional insertion devices of modest length. The corresponding betatron and dispersion functions are plotted in fig. 2. The synchrotron radiation used is produced in the four superconducting bending magnets /6/ and leaves them through outlet slots which run along the outer large circumference. The design values of electron energy, 1.44 GeV, and bending field, 4 T, lead to a characteristic wavelength of 0.2 nm. The circumference of the ring is 33.6 m. Fig. 3 shows an arrangement of 4 scan dipoles producing a closed orbit distortion which is restricted to the region between the outermost pair of scan dipoles except for some small residual deviations due to numerical imperfections. The entrances and ends of the scan dipoles are located at (0.28 m, 0.64 m), (1.40 m, 1.90 m), (6.50 m, 7.00 m), (7.76 m, 8.12 m), respectively. Their maximum strengths are 0.10122 T (#1), -0.10005 T (#2), 0.10005 T, and -0.10122 T, in the same order as above. Compared with earlier work /4/ the number of scan dipoles has been reduced from 6 to 4 at the expense of an increase in the scan field strength. Combinations of more than one cell equipped with scanning are possible, namely, two cells, either adjacent or alternate, three successive cells, or four cells. In these cases, scan dipoles located adjacently in the straight sections might be combined to form only one.

Spatially periodic scan

Though scanning in each cell of the machine can be realized in the way described above using 16 dipoles there are, of course, other ways to do that. One of them uses only 8 dipoles, i.e. two per cell. The corresponding closed orbit distortion is plotted in fig. 4. The first dipole extends from 1.40 m to 1.90 m, the second from 6.50 m to 7.00 m. Their maximum strength is ± 0.084 T (#3). The positions of the remaining six can be calculated using the length of a cell, 8.40 m.

Shift of node

So far, the node of the electron beam is located in the center of the bending magnet. In this case, the vertical amplitudes of the light beams are not evenly distributed along the magnet's outlet slot, as noted by Hagena /7/. However, this distribution can be influenced by shifting the node of the electron beam. Each light beam has its own node which does not coincide with that of the electron beam except for that emanating from the electron beam's node. Instead, the locus of the nodes is a curve which is symmetric to the radius intersecting the closed orbit in the beam node as displayed in fig. 5 a. Fig. 5 b shows a schematic cross-section through the inner part of the magnet to better explain nomenclature. The nodal line is given by the parameter representation

$$\overline{x_n} = \sin\phi + (\phi_o - \phi)\cos\phi$$

$$\overline{y_n} = \cos\phi - (\phi_o - \phi)\sin\phi$$

All quantities with the dimension of a length are normalized to the radius ρ of the closed orbit, e.g., $\bar{x} = x/\rho$ and so forth. ϕ and ϕ_0 are the angles of the tangent point of the light beam considered and of the electron beam node, respectively. The coordinates of the intersection of a light beam with tangent point ϕ with a circle of radius r are

$$\overline{x_r} = \sin\phi + \sqrt{\bar{r}^2 - 1}\ \cos\phi$$

$$\overline{y_r} = \cos\phi - \sqrt{\bar{r}^2 - 1}\ \sin\phi$$

As a consequence, the distance $\overline{\Delta}$ between the node of a light beam and its intersection with the borders r_i and r_a of the outlet slot for the radiation varies and, accordingly, the acceptable angular amplitude of the vertical motion of a light beam. This distance is given by

$$\overline{\Delta} = \left| \phi_o - \phi - \sqrt{\bar{r}^2 - 1} \right|$$

where $\bar{r}$ equals $\bar{r}_i$ or $\bar{r}_a$ depending on which is limiting. For ϕ increasing $\overline{\Delta}$ drops from the value

$$\bar{\Delta}(o) = \phi_o - \sqrt{\bar{r}_i^2 - 1}$$

at $\phi = 0$ to a minimum

$$\bar{\Delta}_{min} = \frac{1}{2}\left(\sqrt{\bar{r}_a^2 - 1} - \sqrt{\bar{r}_i^2 - 1} \right)$$

when the node reaches the circle with radius

$$\bar{r}_{min} = \frac{1}{2} \sqrt{2 + \bar{r}_i^2 + \bar{r}_a^2 + 2\sqrt{(\bar{r}_i^2 - 1)(\bar{r}_a^2 - 1)}}$$

for the first time and rises again to a value of

$$\bar{\Delta}(\phi_m) = \phi_m - \phi_o + \sqrt{\bar{r}_a^2 - 1}$$

Here it is assumed that the last light beam considered intersects the border r_a at the exit of the magnet. The corresponding angle is $\phi_m = \phi_b - \arccos(1/\bar{r}_a)$ with ϕ_b the bending angle and $\phi_m > \phi_o$. The angle ϕ_o is optimum if the values of Δ upstream and downstream are equal. The result is

$$\phi_{o_{opt}} = \frac{1}{2}\left(\phi_m + \sqrt{\bar{r}_a^2 - 1} + \sqrt{\bar{r}_i^2 - 1} \right)$$

For the present magnet design /6/ with $r_a = 1.29$ m, $r_i = 1.24$ m, and $\rho = 1.20$ m $\phi o_{opt} = 0.925 \hat{=} 53°$; magnets with a wedge-shaped cross-section of the outlet slot can be treated by setting $r_a = r_i$. The maximum angular amplitude ψ_{max} of the electron beam can then be calculated using

$$\tan \psi_{max} = \frac{\bar{w}/2 - f\,\bar{\sigma}_L(o) - \bar{\delta y}(o)}{\bar{\Delta}(o)}$$

with the standard deviation $\bar{\sigma}_L$ of the vertical light intensity distribution in the outlet slot estimated for the present case as

$$\bar{\sigma}_L^2(\phi) = \bar{\sigma}_V^2(\phi) + \bar{L}^2\left(\sigma_V'^2(\phi) + \sigma_R^2\right)$$

where $\bar{\sigma}_V$, σ'_V, and σ_R are the standard deviations of the vertical distributions of the positions and the flight direction of the electrons, and of the radiation emitted, respectively, and $\bar{L}$ the normalized distance from the tangent point to the limiting aperture. f is a safety factor re-

minding that one standard deviation might not be enough to obtain a sufficiently small heat load, w is the width of the outlet slot, and δy the vertical closed orbit distortion before scanning, all lengths normalized to ρ as mentioned above. Inserting typical numbers, w = 10 mm, f = 1, σ_R = 0.3 mrad, σ'_V = 0.6 mrad, L = 0.47 m, Δ = 0.8 m, σ_V = 1.3 mm, $\delta y = 0.5$ mm, $\Psi_{max} \cong 4$ mrad is found. Now, the maximum amplitude of the light beams in the outlet slot is equal downstream and upstream which may be desired considering the radiative heat load of the cold magnet bore. However, the amplitude of the electron beam is no longer uniformly distributed which may affect the particle heat load. The compromise may be found experimentally. The node of the distorted closed orbit can be shifted by slightly unbalancing the field strength of the scan dipoles. As an example, the values of the maximum field strength for the node being located at 53° are 0.0815 T and -0.0839 T in the spatially periodic scan mode.

Scan dipoles

* Gap width and vacuum tube aperture

The gap width and the aperture of the vacuum tube are derived from the beam stay clear aperture a_H and a_V, given by

$$a_H = \pm n_H \left(\varepsilon_H \beta_H + (\eta \cdot \delta)^2 \right)^{\frac{1}{2}} + x_o$$

for the horizontal direction (label H), and by

$$a_V = \pm n_V (\varepsilon_V \beta_V)^{\frac{1}{2}} + y_o$$

for the vertical direction (label V), where $n_{H,V}$ are multiples of the standard deviations, $\varepsilon_{H,V}$ the emittances, $\beta_{H,V}$ the betatron amplitudes, η the dispersion, δ the relative energy spread, and x_o, y_o the horizontal and vertical closed orbit deviation. The time-dependent vertical dispersion caused by the scanning dipoles is neglected. The beam stay clear apertures must be evaluated at the locations where they become maximum, i.e., in the middle of the long straight section in the horizontal case, and in the vertically focussing quadrupole in the vertical case. Inserting the numbers for the lattice mentioned above, e.g., $n_H = n_V = 8$, $\varepsilon_H = \varepsilon_V = .333 \times 10^{-6}$ m·rad, β_H = 19.2 m, β_V = 7.9 m,

η = 2.2 m, δ = .001, x_o = 2 mm, y_o = 11 mm, the horizontal and vertical beam stay clear apertures become 28.8 mm and 24.0 mm, respectively. Thus, the clear bore of the vacuum tube should be 60 mm. In order to minimize field distortions due to eddy currents in the wall of the vacuum tube stainless steel bellows will be used in the scan dipoles with an inner and outer diameter of 60 mm and 68 mm, respectively, and a wall thickness of 0.25 mm.

* Shape of the iron yoke

Fig. 6 shows the cross-section through the laminated iron yoke. Its shape, namely, the ratio between the widths of pole piece and leg, is designed to produce a field uniformity of better than 10^{-3} over the beam stay clear aperture. Its length, l_{iron}, derives from the ideal length as quoted above minus an allowance for winding heads and flanges, in our case 12 cm. The magnetically effective length is then calculated from

$$l_{eff} = l_{iron} + 2Kh,$$

K being a form factor of value 0.56 and h the gap width. The effective field strength follows then from equating the field integral Bl calculated using the values of B and l as given above and $B_{eff} l_{eff}$ (Table 1).

* Thickness of laminations

The thickness of the laminated sheaths must be determined from the time-behaviour of the field. Assuming a bipolar triangular temporal variation of the field the corresponding Fourier decomposition is given by

$$B(t) = B_{eff}\left(\frac{8}{\pi^2}\right) \sum_{n=1}^{\infty} \frac{(-1)^{n+1}}{(2n-1)^2} \sin\left[(2n-1)\omega_o t\right]$$

with ω_o the angular scan frequency. Using the skin depth formula

$$d_s^2(n) = \left(0.5 \cdot \omega(n) \cdot \mu_o \cdot \mu_r \cdot \sigma_e\right)^{-1}$$

and admitting higher harmonics up to n = 40 with a frequency-dependent attenuation coefficient A_n for their amplitude /8/

$$A_n = \frac{\sqrt{2}}{x_n} \cdot \left(\frac{\cosh x_n - \cos x_n}{\cosh x_n + \cos x_n} \right)^{1/2}$$

it is found that for d = 0.2 mm thick laminated sheaths the deviation of the true waveform from the ideal triangle can be kept lower than 0.1 % except for a region of about 1 % of the scan period around the apices of the triangles. As usual, μ_o is the permeability of vacuum, μ_r = 3000 the relative permeability of the iron, σ_e = 3 x 10^6 $(\Omega m)^{-1}$ its electrical conductivity, d_s the skin depth, $\omega(n) = n\,\omega_o$, and $x_n = d/d_s(n)$.

* Power supplies and function generators

The power supplies must provide the inductive voltage

$$U_L = LdI/dt = (2/\pi) \cdot L \cdot I_{max} \cdot \omega_o,$$

and the resistive voltage

$$U_R = RI_{max},$$

with L the inductance, R the resistance, I_{max} the maximum current. The time-dependence of current and voltage is plotted schematically in fig. 7. The electrical power will come from commercial power supplies based on a fast transistor bridge as developed by /9/. They will be controlled by freely programmable function generators with a time and amplitude resolution of 10 µs and 0.1 % of maximum amplitude as developed at BESSY. The main scan dipole data are summarized in Table 1.

Table 1: Main scan dipole data

		#1	#2	#3
B_{eff}	(T)	.115	.110	.092
l_{iron}	(m)	.24	.38	.38
Ampereturns	(A)	6233	5952	4951
Number of loops		24	24	24
Inductance L	(mHy)	.60	.87	.87
Maximum current	(A)	260	248	206
Effective current	(A)	150	143	119
Effective current density	(A/mm^2)	1.88	1.79	1.49
Resistance R	(mΩ)	5.3	6.6	6.6
L/R	(s)	.11	.13	.13
Inductive voltage U_L	(V)	62.4	85.8	71.3
Resistive voltage U_R	(V)	1.4	1.64	1.36

Lifetime reduction

Since the scanning brings the beam periodically closer to a limiting aperture those lifetimes which depend on an aperture are expected to be reduced. As a model the periodic vertical motion of the beam is replaced by an oscillation of an aperture as sketched in fig. 8. For simplicity, only the fundamental of the Fourier decomposition is taken into account, however with the full amplitude so that the lifetime reduction is overestimated. The time-averaged lifetime τ_k is defined as

$$\tau_k = 1/(\langle 1/\tau(x(t))\rangle)$$

where $\langle\rangle$ stands for time-averaging and x(t) for the aperture. In case of the quantum lifetime τ_q, the well known formula

$$\tau_q = (\tau_H/2)(\exp(\xi)/\xi)$$

with $\xi(t) = 0.5(x(t)/\sigma)^2$ and τ_H the horizontal damping time leads to

$$\langle 1/\tau_q(x(t))\rangle = (8/T\tau_H)\int_0^{T/4} \xi \exp(-\xi)\, dt$$

The integral is evaluated numerically. As fig. 9 shows the resulting quantum lifetime with scan is smaller than that without scan by many orders of magnitude, but still greater than that corresponding to the minimum distance between distorted closed orbit and aperture. The Coulomb lifetime is given in literature /10/ by

$$\tau_c = C_1(Ex(t))^2/(p\beta_o\langle\beta\rangle),$$

with E the electron energy in GeV, p the average pressure in nTorr, β_o the betatron amplitude at the position of the aperture, $\langle\beta\rangle$ the average betatron amplitude, both in m, and the constant $C_1 = 1.0 \times 10^7$ h/GeV^2 nTorr. In the same way as above one obtains

$$\frac{\tau_{ck}}{\tau_c} = \frac{\pi}{2}(1-y^2)\left[\frac{2}{\sqrt{1-y^2}}\left(\arctan\left(\frac{1-y}{1+y}\right)^{\frac{1}{2}} + \arctan\frac{y}{\sqrt{1-y^2}}\right) + y\right]^{-1}$$

with $y = a/x_o$. Using E = 1.435 GeV, σ = 1.3 mm, p = 1 nTorr, β_o = 8 m, and $\langle\beta\rangle$= 5.5 m, the results plotted in fig. 10 indicate also a significant

reduction due to the scan. However, the effective lifetime τ resulting from

$$1/\tau = 1/\tau_{ck} + 1/\tau_{qk}$$

is sufficiently long ($>10^5$ s) provided the minimum distance between aperture and distorted closed orbit exceeds 6 standard deviations. This requirement is met by the vacuum tube offering a beam stay clear aperture of ± 8 standard deviations.

Conclusion

The design of an electron beam scanning system described above appears technically feasible and compatible with storage ring operation. It offers unusually large ranges of both scan amplitude and frequency, and some freedom to choose the location of the scan in the machine. Its practical operation should allow to optimize scan parameters with respect to target irradiation as well as to storage ring performance and to find out limits, in particular, in the case of curved superconducting bending magnets with a cold bore for which practical experience is still lacking.

Acknowledgment

Useful discussions with J. Mohr and D. Münchmeyer as well as critical remarks by O.F. Hagena are gratefully acknowledged.

References

/1/ G. Mülhaupt et al., IEEE Transactions on Nuclear Science NS-32(5), 3368-3370(1985).

/2/ T. Tomimasu, T. Noguchi, S. Sugiyama, T. Yamazaki, T. Mikado, IEEE Transactions on Nuclear Science NS-32(5), 3403-3405(1985).

/3/ E.W. Becker, W. Ehrfeld, D. Münchmeyer, Kernforschungszentrum Karlsruhe, Report KfK 3732, April 1984.

/4/ D. Einfeld, O.F. Hagena, P.R.W. Henkes, R. Klingelhöfer, B. Krevet, H.O. Moser, G. Saxon, G. Stange, Kernforschungszentrum Karlsruhe, Report KfK 3976, September 1985.

/5/ E. W. Becker, W. Ehrfeld, P. Hagmann, A. Maner, D. Münchmeyer, Microelectronic Engineering 4, 35-56(1986).

/6/ B. Krevet, H.O. Moser, C. Dustmann, in Advances in Cryogenic Engineering, Vol. 33, R. W. Fast, ed., Plenum Publishing Corporation, 1988, pp. 25-32.

/7/ O.F. Hagena, 1985, unpublished.

/8/ K. Küpfmüller, Einführung in die theoretische Elektrotechnik, Springer, Berlin, 1984.

/9/ G. Breitenberger, R. Steiner, Gesellschaft für Schwerionenforschung, Darmstadt, GSI Report 309, 1983.

/10/ H. Wiedemann, Report ESRP-IRM-10/83, European Synchrotron Radiation Facility, 1983.

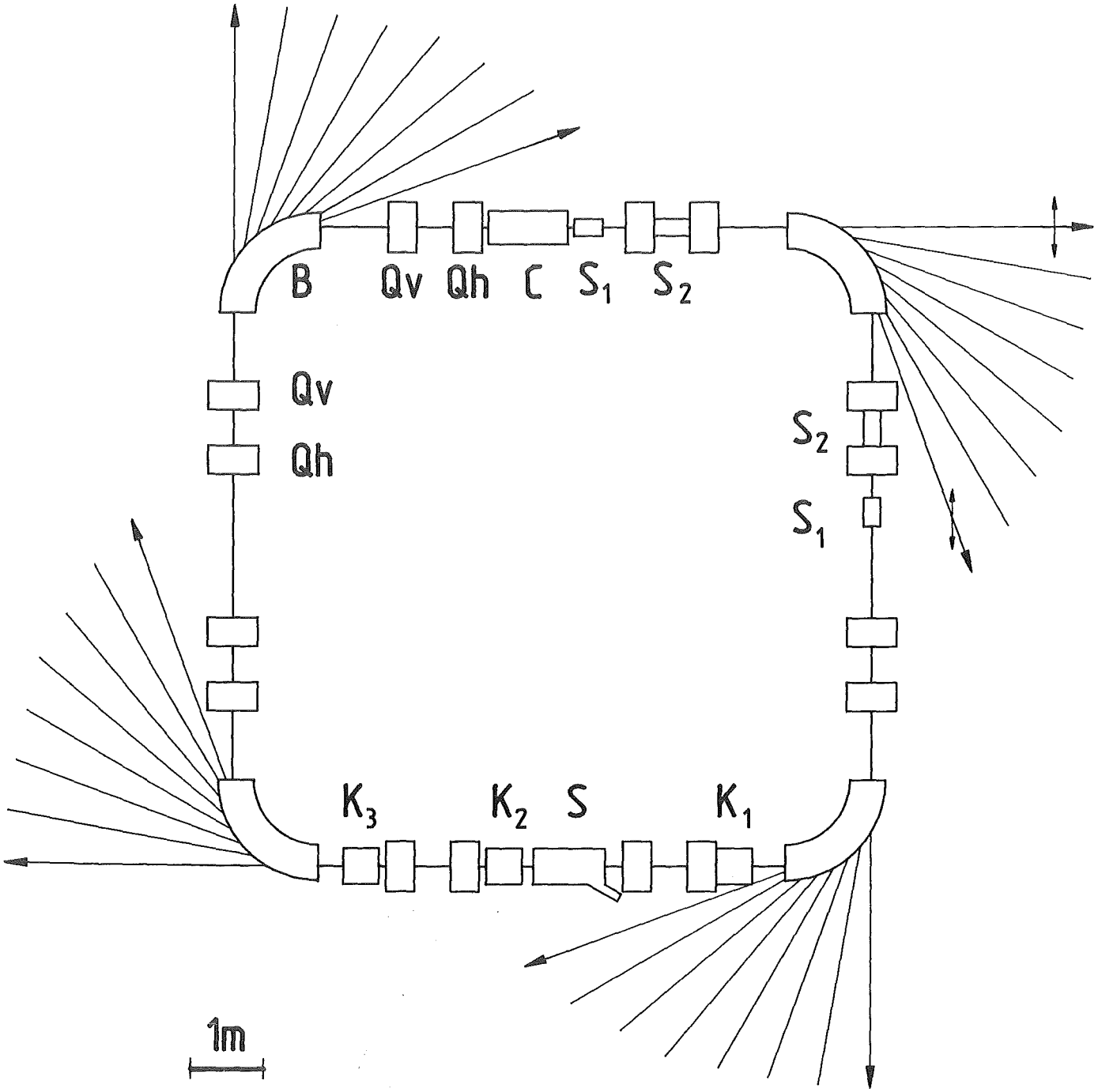

Fig. 1: Lattice of KSSQ (B superconducting bending magnet, Qh, Qv horizontally and vertically focusing quadrupoles, C RF cavity, $S_{1,2}$ scan dipoles, K_{1-3} injection kickers, S septum)

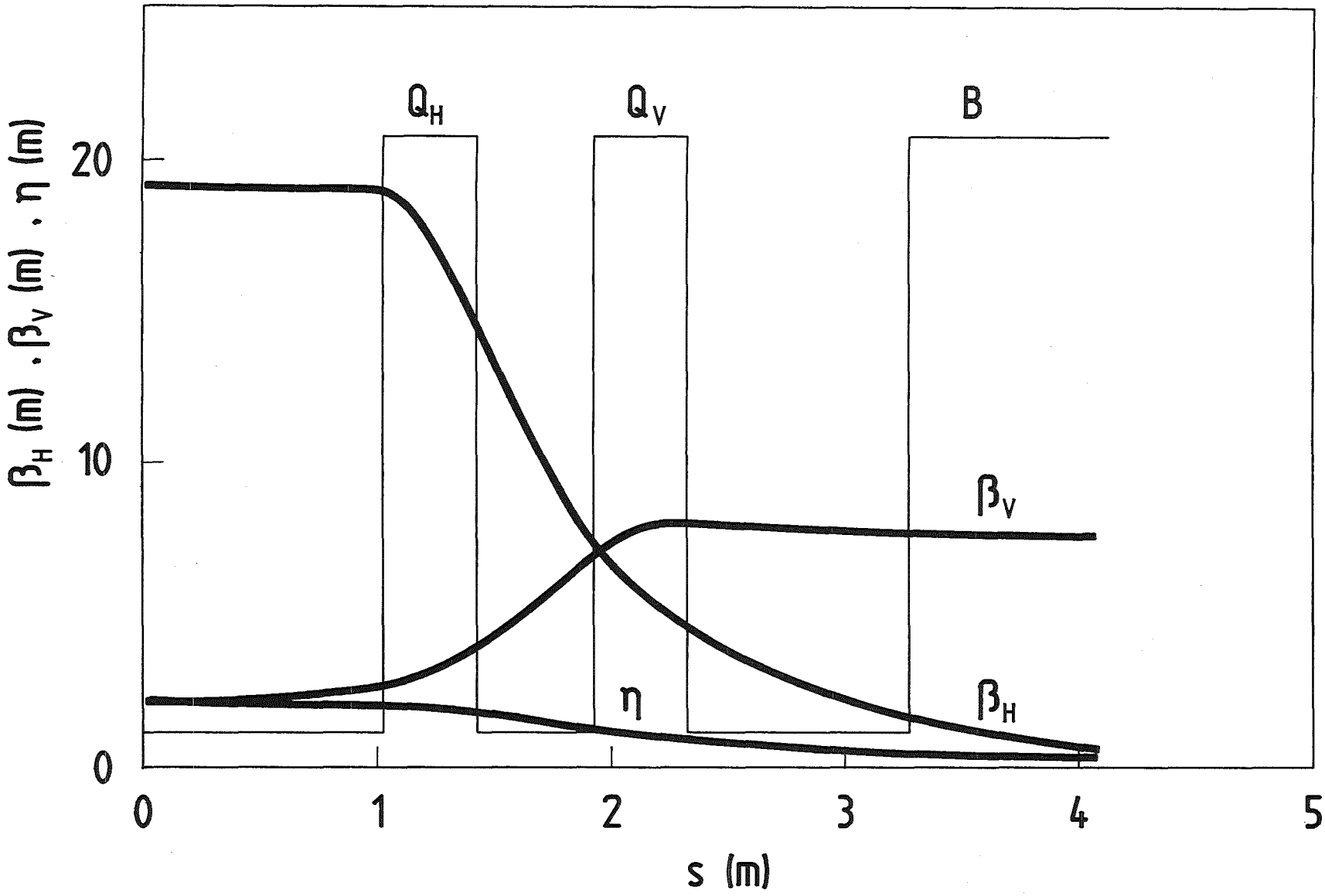

CAD KfK L-K3.491.888 IKVT

Fig. 2: Betatron and dispersion functions

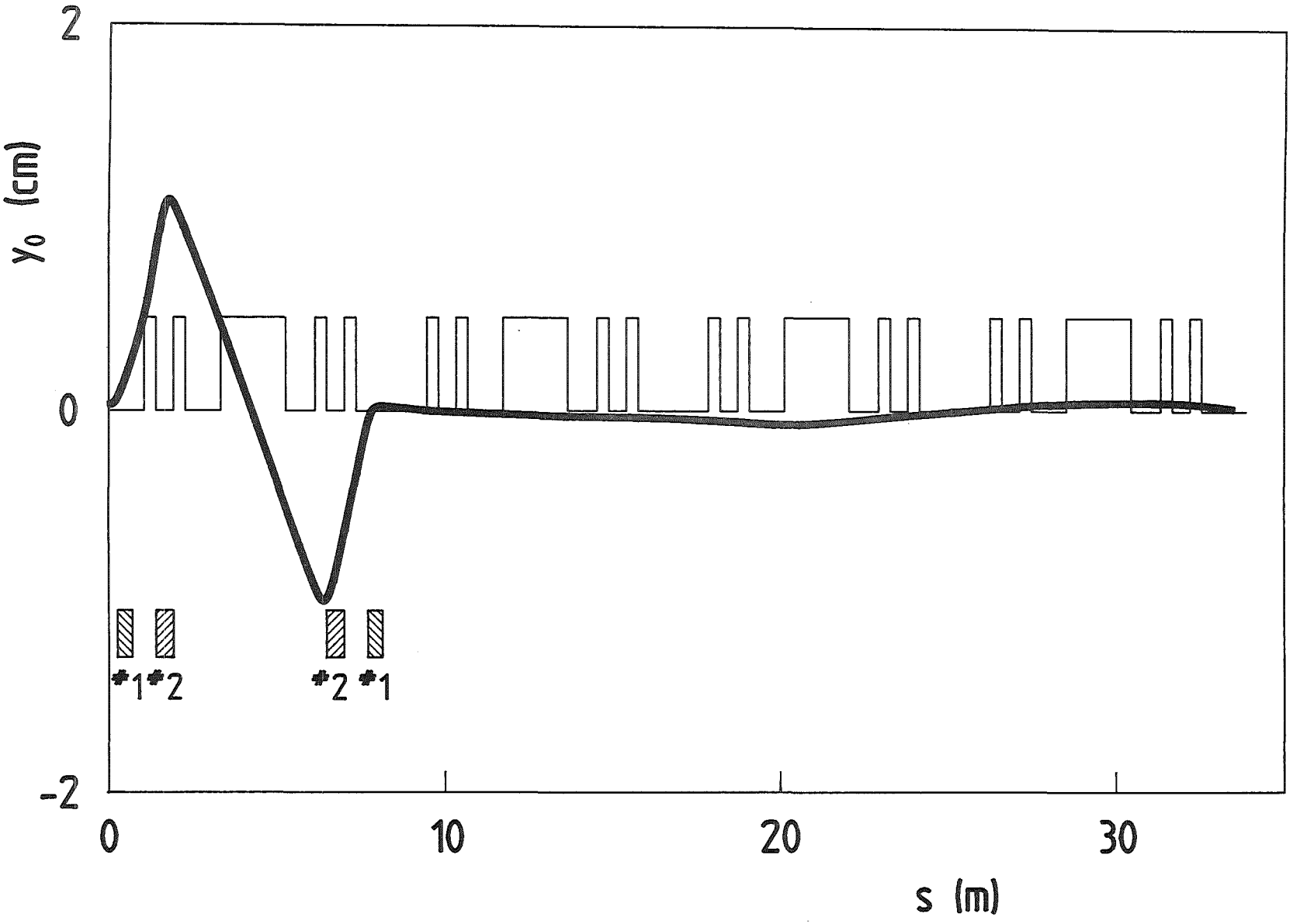

CAD KfK L-K3.489.888 IKVT

Fig. 3: Closed orbit distortion and arrangement of four scan dipoles in the case of scanning restricted to one cell.

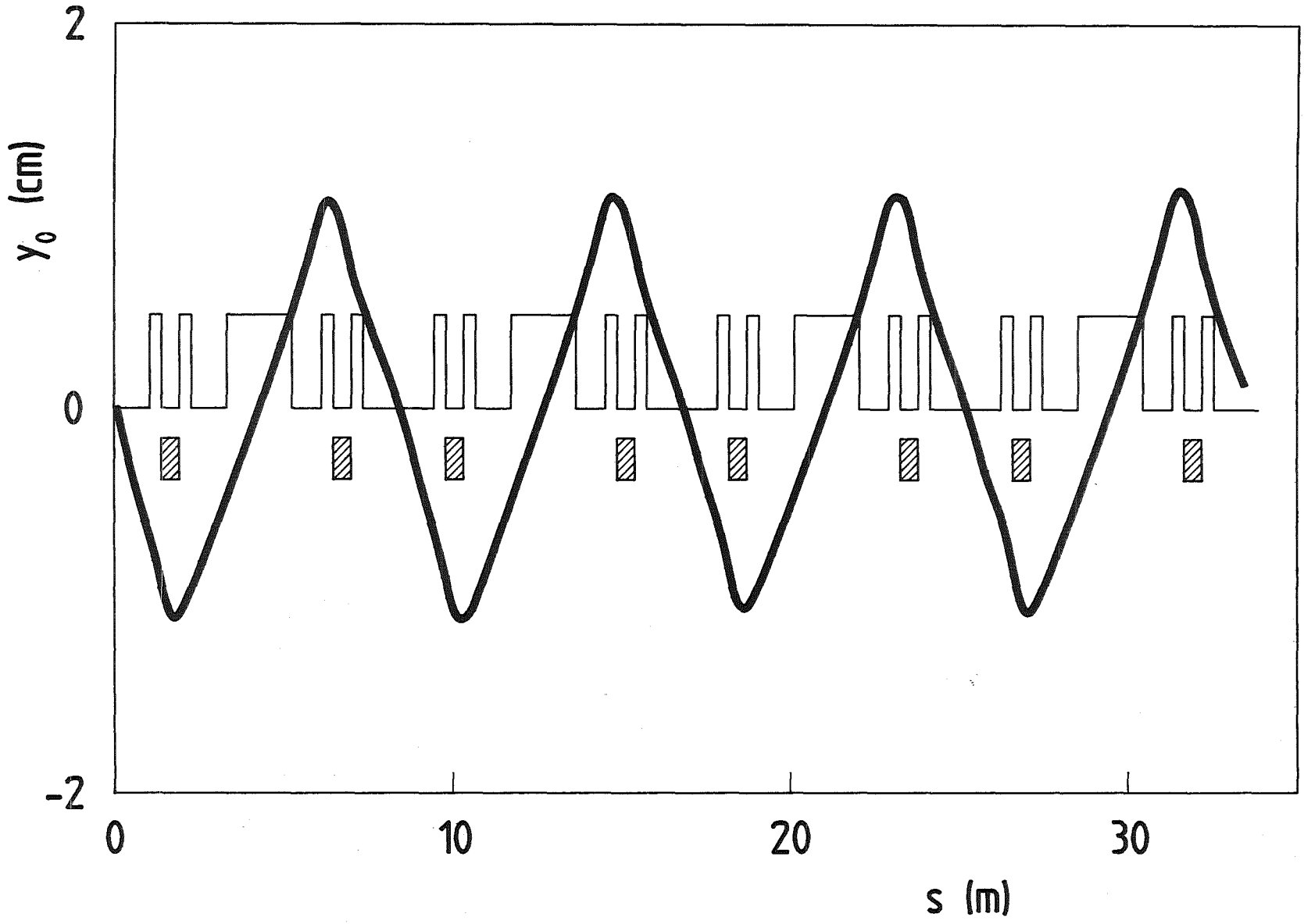

CAD KfK L-K3.490.888 IKVT

Fig. 4: Closed orbit distortion and arrangement of eight scan dipoles for spatially periodic scanning along the whole circumference.

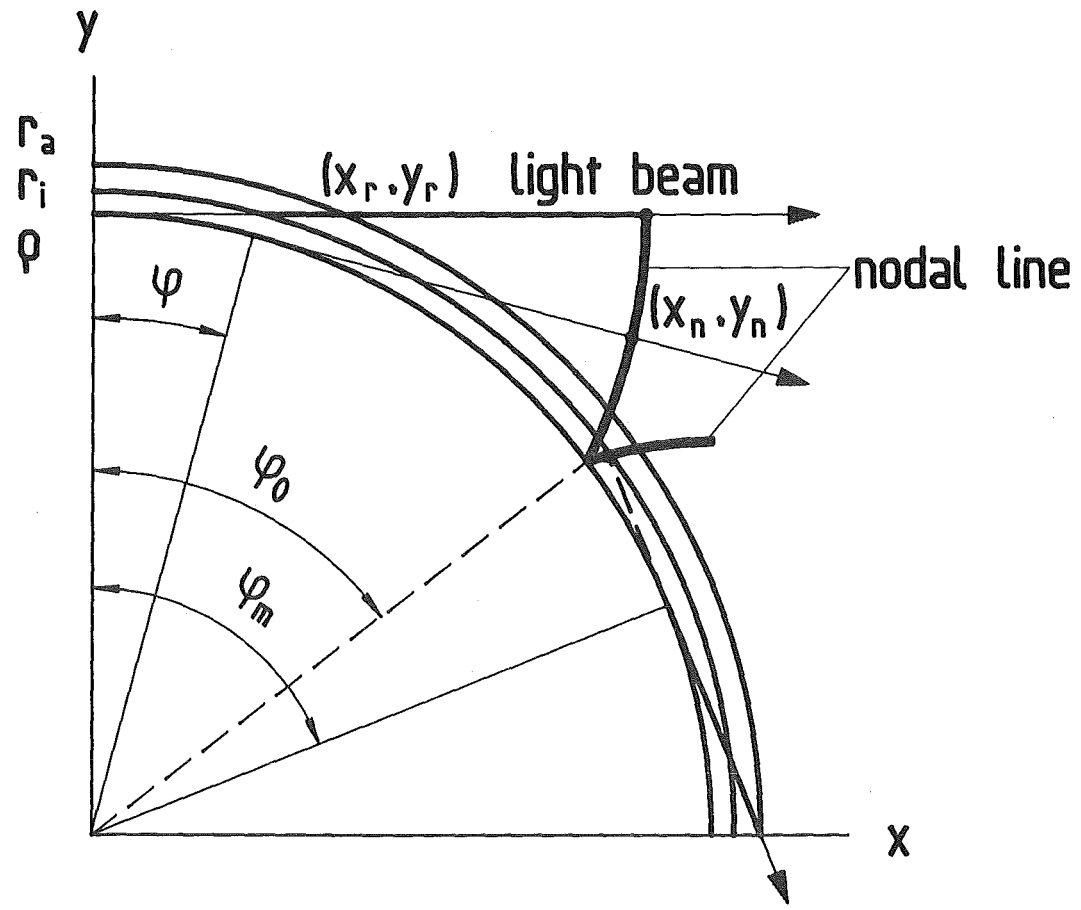

a)

Fig. 5a): Locus of nodes of the light beams.

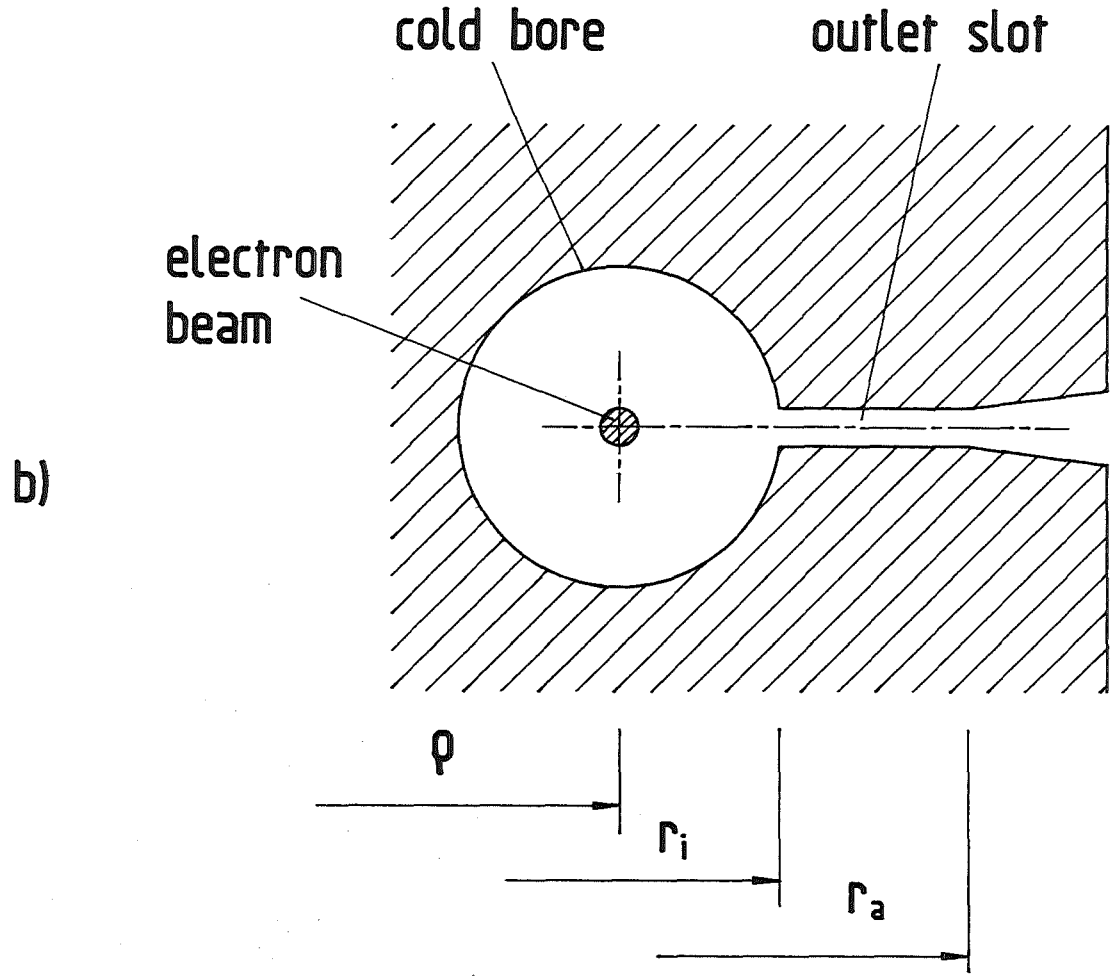

Fig. 5b): Schematic cross-section through inner part of bending magnet.

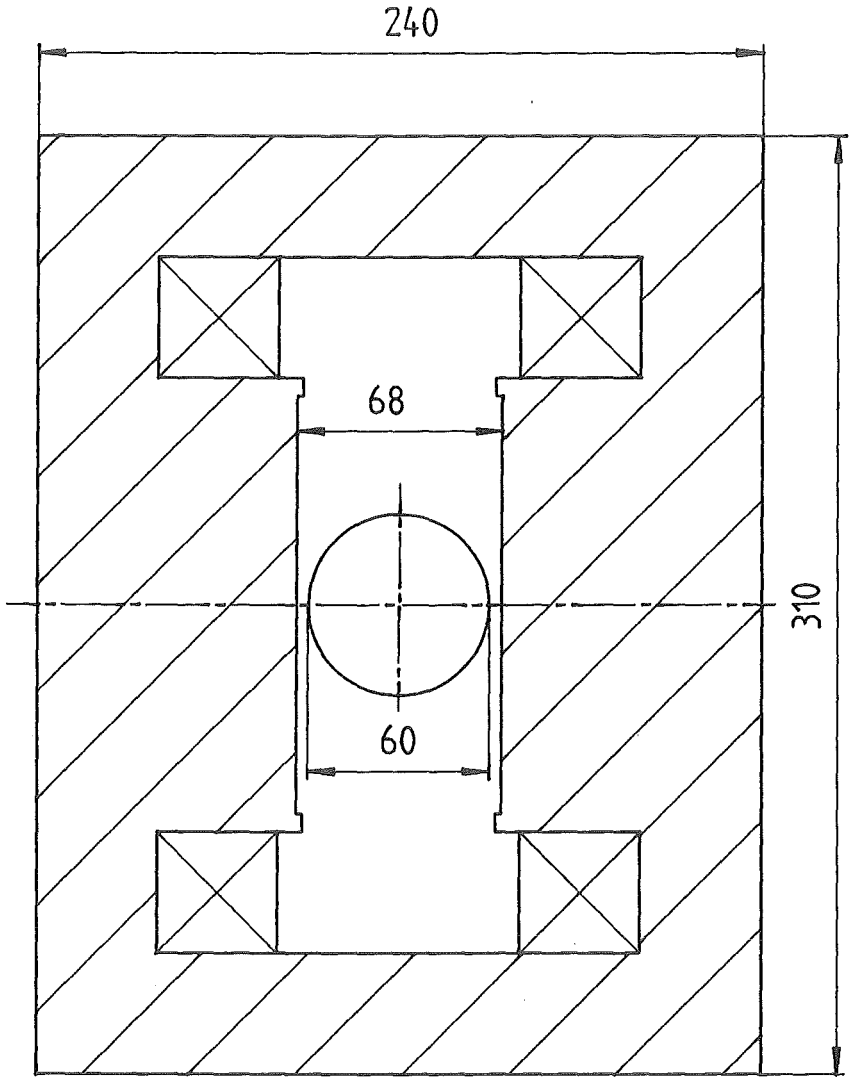

Fig. 6: Cross-section through iron yoke of scan dipoles.

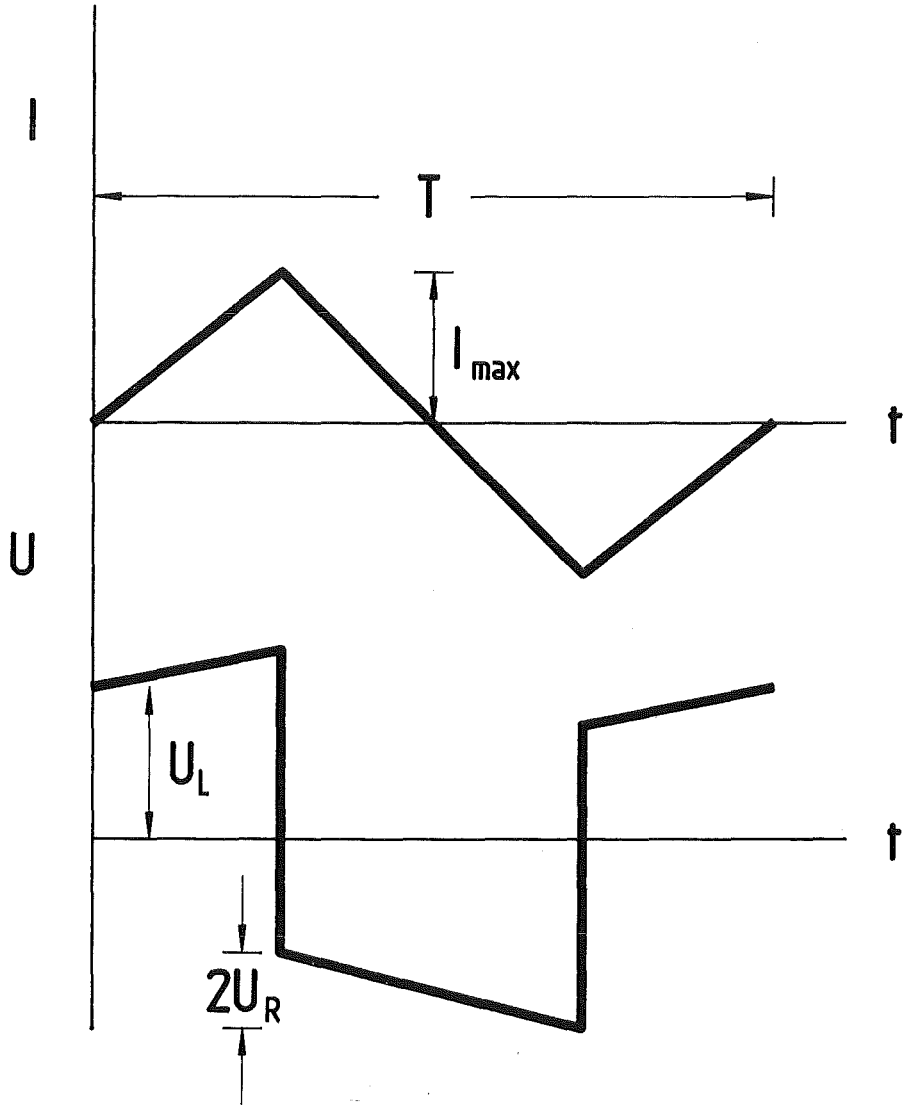

Fig. 7: Schematic plot of current and voltage versus time.

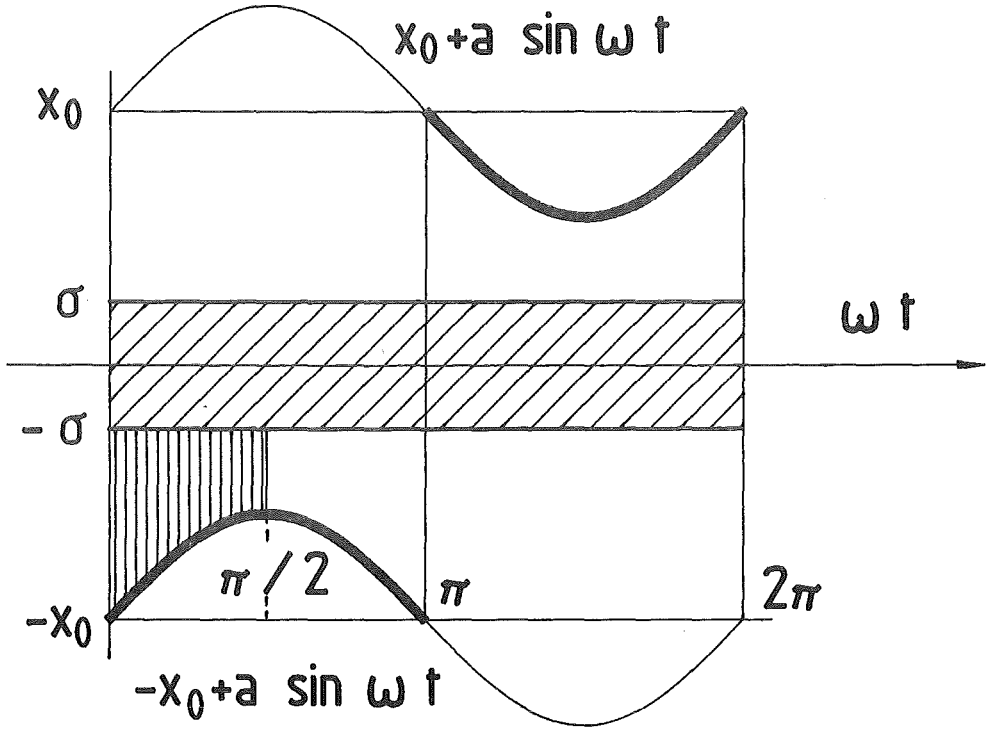

Fig. 8: Aperture variation replacing the scan of the beam.

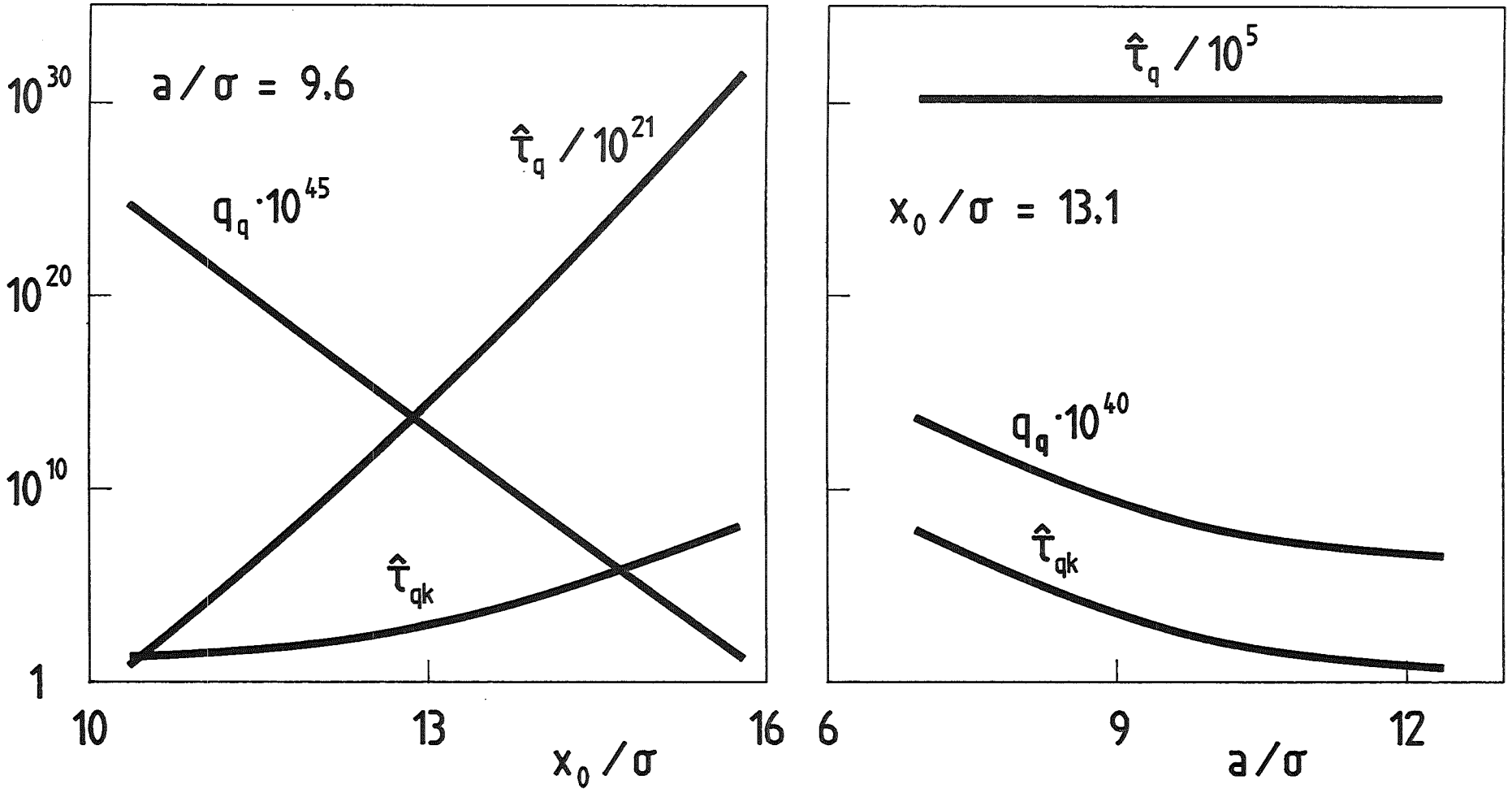

Fig. 9: Quantum lifetime, normalized to half the horizontal damping time, with scan $\hat{\tau}_{qk}$ and without $\hat{\tau}_q$, and ratio of both q_q, versus aperture x_o/σ at constant scan amplitude, and versus scan amplitude a/σ at constant aperture (σ 1.3 mm).

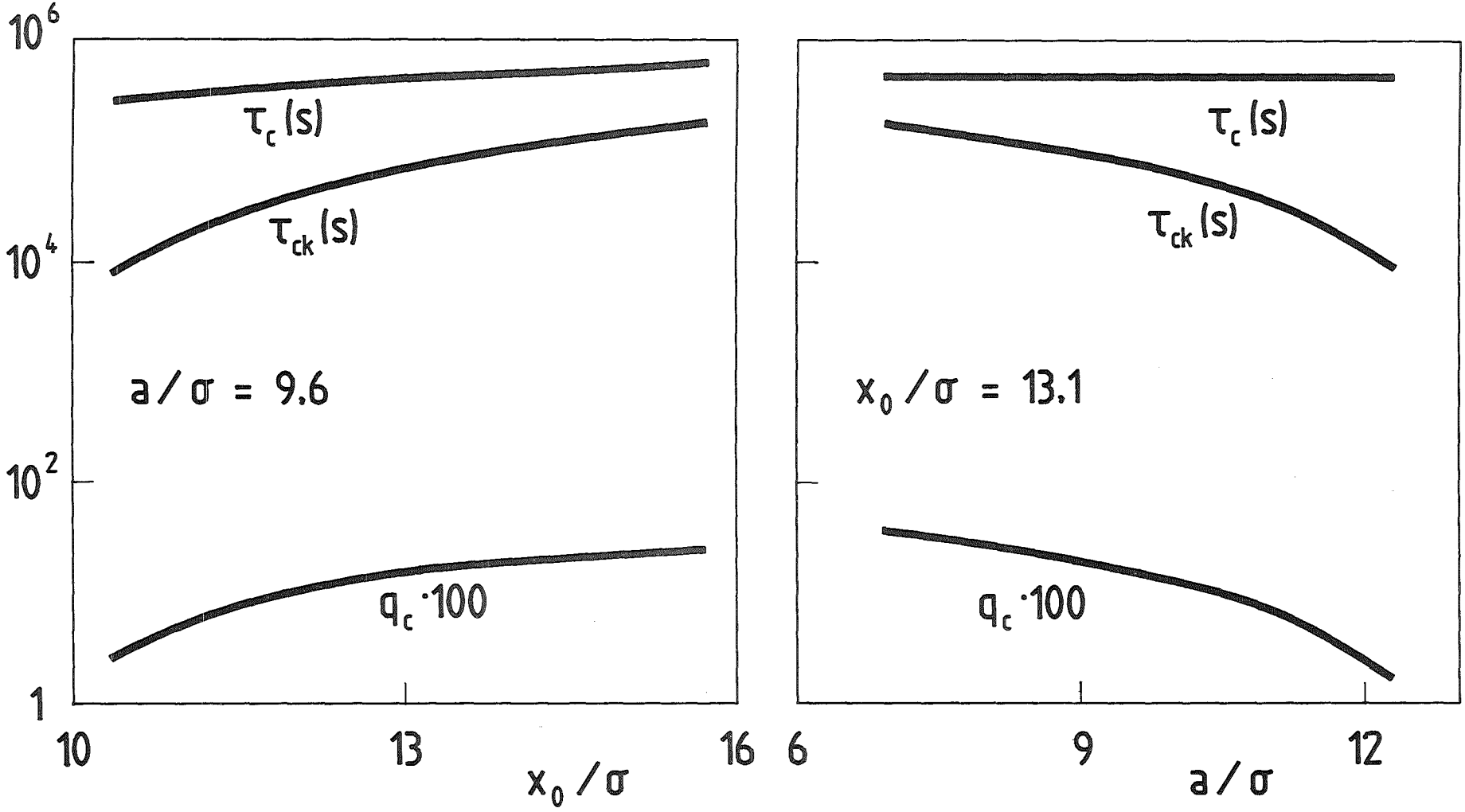

Fig. 10: Coulomb lifetime, with scan τ_{ck} and without τ_c and ratio of both q_c, versus aperture x_o/σ at constant scan amplitude, and versus scan amplitude a/σ at constant aperture (σ 1.3 mm, β_V 8 m, $\langle\beta_V\rangle$ 5.5 m).